Results in Materials 28 (2025) 100825

Contents lists available at ScienceDirect

Results in Materials

journal homepage: www.sciencedirect.com/journal/results-in-materials

Optimization of the electrical and dielectric properties of Zn-doped ferrites: Insights into the temperature-dependent behavior and applications in advanced electronics

Sadiq H. Khoreem [a,b,*], A.H. Al-Hammadi [c]

[a] Department of Optometry and Vision Science/Faculty of Medical Sciences, Al-Razi University, Sana'a, Yemen
[b] Center of Research and Studies, Amran University, Amran, Yemen
[c] Physics Department/Faculty of Science, Sana'a University, Sana'a, Yemen

ARTICLE INFO

Keywords:
Barium hexaferrite innovation
Energy-efficient technologies
Eco-friendly functional materials
Electrical performance optimization
Green production

ABSTRACT

This study investigated the role of zinc (Zn) substitution on the electrical and dielectric behavior of $BaNi_{1-x}Zn_xFe_{16}O_{27}$ W-type hexaferrites for AC electrical conductivity (σ_{ac}), dielectric constant, and structure properties with (x = 0.0–2.0). High-purity oxides were blended and sintered by the ceramic process, and the measurements were carried out over the frequency range of 1–100 kHz and temperature range from room temperature to 500 °C using a Wayne Kerr 6500P LCR meter. The samples exhibited semiconducting activity, with σ_{ac} increasing at elevated temperatures owing to the thermally activated charge carriers. The observed transition temperature for samples with x = 1.6 and x = 2.0 reflects a conduction mechanism transition shift, whereas the wide tan δ peaks at these levels disclose complex dielectric relaxation responses. In addition, the broad peaks in the tan δ, spectrum at these levels reveal the complex dielectric behavior and frequency-dependent relaxation processes. The behavior at x = 1.6 and x = 2.0, is an unrivaled combination of electrical conductivity and complex dielectric properties, which offers pathways for tailoring materials for high-temperature and frequency-sensitive applications. The single-phase W-type hexaferrite frame was verified through X-ray diffraction (XRD) analysis, with expanding lattice parameters as larger Zn^{2+} cations replaced smaller Ni^{2+} cations. Microstructural studies have shown that minimal grain growth and porosity increase with Zn content, which are characteristics that determine charge transportation, and polarization. Optimized behaviors were achieved for x = 0.4, with the maximum σ_{ac} and ε' and the lowest tan δ, proposed as a consequence of the optimal Fe^{2+}/Fe^{3+} hopping and polarization mechanisms. The results attest that Zn substitution efficiently tunes the structural, electrical, and dielectric parameters of $BaNi_{1-x}Zn_xFe_{16}O_{27}$ ferrite and can be used for advanced applications as a superior material for radio-frequency and microwave devices, capacitors, materials innovation, and energy-storage applications.

1. Introduction

Ferrite materials have garnered significant attention owing because of their broad applicability in modern technologies, including microwave devices, magnetic recording systems, and electromagnetic wave absorbers [1–4]. Among these ferrite materials, barium hexaferrites have long been recognized as vital materials in advanced technology and stand out for their superior magnetic and dielectric properties, high chemical stability, strong magnetic anisotropy, and low electrical losses [5,6]. These characteristics make these materials particularly suitable for advanced applications in the fields of electronics, energy storage, and environmental engineering [7]. In addition, these properties can be drastically modified by doping with magnetic, nonmagnetic, or rare-earth ions, such that new applications can be designed, and the functional ability of the material can be broadened. Hence, a vast amount of research has focused on doping methods to enhance the properties of barium hexaferrite [8–15]. Despite these advancements, barium ferrites still possess electrical conductivity and dielectric drawbacks, that restrict their application in high-efficiency devices. These drawbacks are predominantly caused by the high resistivity and low tenability of dielectric constants at varying frequencies [16]. The lack of free charge carriers and inhibition of ionic and electronic mobility also

* Corresponding author. Department of Optometry and Vision Science/Faculty of Medical Sciences, Al-Razi University, Sana'a, Yemen.
E-mail address: khoreems@yahoo.com (S.H. Khoreem).

https://doi.org/10.1016/j.rinma.2025.100825
Received 14 February 2025; Received in revised form 5 October 2025; Accepted 18 November 2025
Available online 19 November 2025

limit their application in technologies such as wearable electronics and high-performance sensors [14,17]. To overcome these challenges, doping strategies have been explored, with zinc (Zn) and nickel (Ni) emerging as effective dopants for enhancing the structural, electrical, and dielectric properties [11]. Among these, Zn doping has shown exclusive potential through the mechanism of resistivity reduction through the creation of localized energy states that enable electron hopping, thereby reducing the energy barrier for charge transfer through the Fe^{3+}-O-Fe^{3+} pathways [18–20]. These modifications enhance the electrical conductivity and improve the dielectric properties, such as the dielectric constant, and reduce loss across a large frequency range; hence, Zn-doped ferrites have potential applications at high frequencies [14,21,22]. Moreover, Zn doping alters the microstructure and improves the charge carrier mobility and polarization mechanisms; however, a balance must be reached from the point of view of structural stability against improved functional performance. Nickel doping complements these effects by optimizing grain boundaries and reducing porosity, thereby facilitating better charge transport and enhancing material densification, which are crucial for energy storage applications [23,24]. Ni doping also stabilizes the dielectric behavior under various environmental conditions by enhancing the dipole relaxation processes and modifying the Curie temperature and magnetic coupling, indirectly influencing the dielectric stability [11,25,26]. The combined effects of Zn and Ni doping not only improve the electrical and dielectric properties but also enhance the magnetic and optical characteristics, as Zn lowers the crystal anisotropy to support microwave absorption and photonic applications, and Ni contributes to better magnetic ordering for multifunctional devices [13,27–29]. The combination of Ni and Zn dopants improves the performance of ferrite materials, particularly in energy storage and magnetic recording applications. Their interactions improve the magnetic and electrical properties owing to increased permeability, reduced magnetic losses, and enhanced conductivity. These developments make Ni-Zn ferrites highly desirable in inductive applications and high-frequency devices, where they provide stable performance, minimum energy dissipation, and efficient signal transmission in tune with modern technological demands [15,18,30,31]. Although previous studies have highlighted the benefits of Ni and Zn doping in ferrites, there is a lack of comprehensive analysis of their combined effects and optimal Zn doping levels in barium ferrites, particularly regarding the interplay between the dielectric and electrical properties as functions of temperature, frequency, and composition. In this study, Zn-doped ferrites were investigated in order to optimize their dielectric and electrical properties. Zn doping is known to enhance polarization mechanisms and reduce energy dissipation, providing advantages in dielectric performance over Ni-doped systems, which primarily focuses on magnetic enhancement.

Therefore, the present study addresses these aspects by investigating the effects of Zn substitution on the electrical and dielectric properties of barium-nickel ferrite. Important characteristics, such as AC electrical conductivity (σ_{ac}), loss tangent (tan δ), permittivity constant (ε', ε''), and structural properties were investigated as functions of Zn substitution at different frequencies and temperatures. This study aimes to determine the doping level that optimizes the performance and understands temperature-dependent behaviors. Focusing on the study of Zn-doped barium-nickel ferrites, this research contributes to the field by providing an overview of their application potential in RF and microwave devices, capacitors, and energy storage systems, furthering advances in high-performance materials for state-of-the-art technologies.

2. Synthesis and experimental procedure

In this work, polycrystalline samples of $BaNi_{2-x}Zn_xFe_{16}O_{27}$ ferrites (with x varying from 0.0 to 2.0) were synthesized using high-purity raw materials: ferric oxide (Fe_2O_3), the carbonate of barium ($BaCO_3$), the oxide of zinc (ZnO), and oxide of nickel (NiO). The starting powders were weighed according to their molecular weight ratios to achieve the desired stoichiometries as indicated in Table 1. The synthesis followed the chemical reaction equation (1):

$$BaCO_3+(2-x)\ NiO + xZnO+8Fe_2O_3 \rightarrow BaNi(2\text{-}x)\ ZnxFe_{16}O_{27}+CO_2\uparrow \quad (1)$$

The molecular weight ratios of the raw materials used for synthesizing $BaNi_{2-x}Zn_xFe_{16}O_{27}$ ferrites are presented in Table 1. These values were calculated based on the molar masses of $BaCO_3$ (197.34 g/mol), NiO (74.69 g/mol), ZnO (81.38 g/mol), and Fe_2O_3 (159.70 g/mol), and normalized per formula unit of $BaNi_{2-x}Zn_xFe_{16}O_{27}$. The same approach was reported in our earlier work [27], and the present table was reproduced to ensure transparency and reproducibility in the current study.

The values in Table 1 were reproduced from our previous work [27], in which detailed step-by-step calculations were provided.

A ceramic technique was used for sample preparation. Initially, the raw materials were mixed and ground for 6 h in an agate mortar and then mechanically grinding for 5 h to ensure a uniform mixture. After 5 h of pre-sintering in air at 1170 ± 10 K, the resultant powder mixtures were gradually cooled to room temperature. The pre-sintered powders were reground for three additional hours to achieve a fine particle size and homogeneity. The powdered materials were compressed into disc-shaped pellets with a diameter of 1.5 cm as well as a thickness of 0.3–0.6 cm using a uniaxial pressure of 10 tons/cm^2 to perform electrical testing. After 4 h of sintering at 1250 K, each sample was gradually cooled to the ambient temperature. Powder samples were prepared for XRD measurements,and the disc surfaces were polished to achieve smooth and parallel faces, and a thin layer of silver paste was applied to both sides to serve as electrodes for electrical testing. Fig. 1 shows a flowchart of the production synthesis method.

Characterization: To comprehensively examine the influence of Zn substitution on the structural, and electrical properties of barium ferrite nanoparticles, a suite of analytical techniques was utilized.

An LCR meter (Wayne Kerr 6500P) was used to calculate the AC electrical conductivity (σ_{ac}), the dielectric constant (ε', ε''), and the dielectric loss tangent (tan δ). To assess the frequency and temperature-dependent behavior of the samples, these measurements were conducted over a frequency range of 1–100 kHz and a temperature range of room temperature (RT) to 500 K. A Shimadzu EDX-720 X-ray diffractometer with Cu Kα radiation (λ = 1.5406 Å) was employed to determine the crystal structure, and phase composition of the synthesized $BaNi_{2-x}Zn_xFe_{16}O_{27}$ ferrites. The XRD patterns were collected over a 2θ range of 5°–75° at a step size of 0.02°/s. Preparative and measurement methods have been used very accurately and reliably for studying Zn-doped ferrites both XRD, both dielectrically and electrically, to draw valuable inferences about their behavior and application performance.

3. Results and discussion

3.1. AC electrical conductivity

Conductivity in the AC electric of Zn-doped barium ferrites was measured at varying concentrations of Zn ions in terms of temperature for the frequency regime 1–100 kHz. Fig. 2 depicts the dependence of the log of the AC conductivity (log σ_{ac}) on the reciprocal temperature (1000/T) for x = 0.0–2.0 compositions. As indicated in Fig. 2, all the samples display semiconducting character: σ_{ac} rises with temperature due to thermally activated hopping of charge carriers from/into the Fe^{2+} and Fe^{3+} ions, in accordance with conduction mechanisms documented in Zn-substituted ferrites [32,33].

At low temperature, σ_{ac} is small and frequency-dependent due to the limitation of mobility from scattering and misalignment of carriers at grain boundaries. With rising temperature, σ_{ac} increases sharply due to the liberation of trapped carriers and the increase in hopping of Fe^{2+}/Fe^{3+}. Further assistance is provided at higher temperature due to increased lattice vibrations, which bring ions in their vicinity more close

Table 1
Molecular weight ratios of the raw materials used to synthesize $BaNi_{2-x}Zn_xFe_{16}O_{27}$ ferrites (x = 0.0–2.0).

Elements		Composition	Total Molecular weights	weight of oxides in grams				Total weight of composition (30 g)
–	Molecular weights	Empirical Formula	g/mole	BaCo3	(NiO)2-x	8(Fe2 O3)	(ZnO)x	
Zn	65.38	BaNi2 Fe16 O27	1672.306	3.540286	2.679859	23.77986	0	30
C	12.011	Ba Ni1.6 Zn0.4 Fe16 O27	1674.98	3.534632	2.140464	23.74188	0.583021	30
O	15.999	Ba Ni**1.2** Zn**0.8** Fe16 O27	1677.655	3.528997	1.602789	23.70403	1.164182	30
Ni	58.693	Ba Ni**0.8** Zn**1.2** Fe16 O27	1680.33	3.52338	1.066825	23.6663	1.743494	30
Fe	55.85	Ba Ni**0.4** Zn**1.6** Fe16 O27	1683.004	3.517781	0.532565	23.62869	2.320964	30
Ba	137.34	Ba Zn**2** Fe16 O27	1685.679	3.512199	0	23.5912	2.896601	30

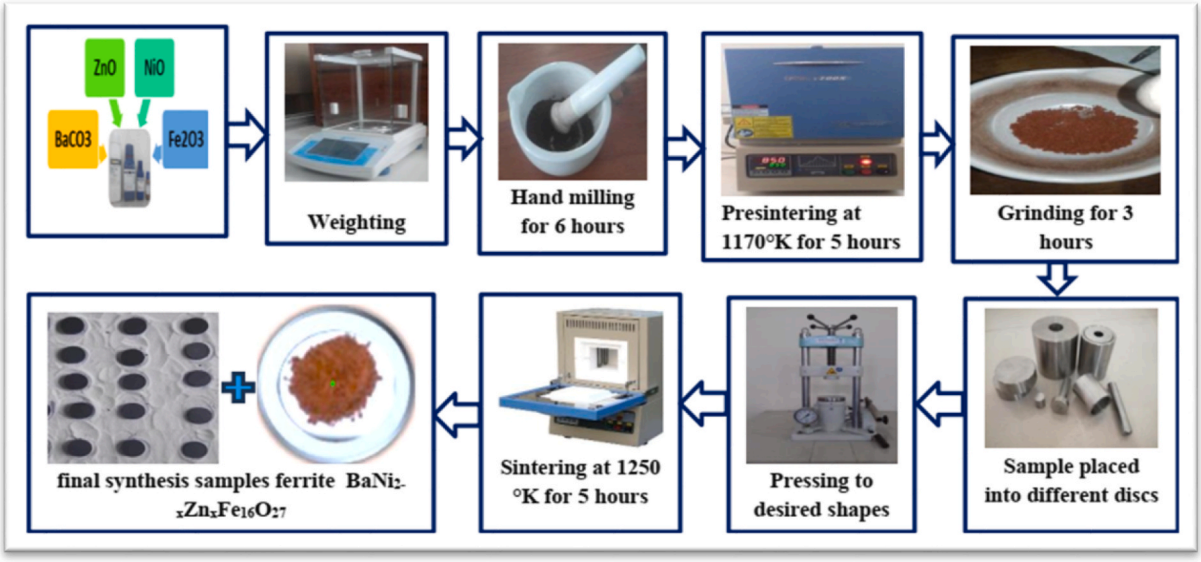

Fig. 1. Schematic flowchart of the $BaNi_{2-x}Zn_xFe_{16}O_{27}$ ferrite preparation route via the ceramic technique.

and increase carrier mobility [34]. Thus, the curves show linear Arrhenius-type dependence (log $\sigma_{ac} \propto 1/T$) at temperature below a characteristic transition temperature, Tσ, vindicating thermally activated transport. Analogous temperature-induced conductivity increase below Tσ is universal for ferrites, in which σ_{ac} increases due to thermally assessed electron exchange among near-neighbor cations possessing mixed-valence [32,34].

Compare to that, at high temperature (T > Tσ), σ_ac slows down gradually for all the samples: the curves bend away from linear and exhibit less steep slope or slight slope downward, more pronounced for x = 1.6 (Fig. 2e) and x = 2.0 (Fig. 2f). This is due to increased thermal motion and phonon scatting, which disorient the orientation of hopping carriers and decrease their effective mobility and thus raise up their conductivity. Further, σ_{ac} rises with frequency, indicating larger carrier mobility and potential tunneling assistance at higher frequency—an observation that the majority conduction mechanism may change with frequency [35,36]. The transition temperature measured for x = 1.6 and 2.0 is an essential point beyond which the prevailing conduction mechanism is altered. Below T < Tσ, heat energy daligns carriers from the applied field and aids electron hopping; above T > Tσ, thermal motion disrupts this alignment, causing conductivity to decrease. Experimentally, Tσ is a handy criterion for maximizing materials performance in temperature-dependent applications (e.g., temperature sensors and resistive elements). Generally, σ_{ac} (T) has two regions defined apart by Tσ. The increase in Tσ to higher temperature with increasing Zn content indicates that Zn addition pinnings the conduction pathway, causing the onset of the conductivity depression due to disorder delay.

3.2. Real part of the complex permittivity (ε`)

The real part of the complex permittivity ε' for the Zn-doped ferrites was measured in the frequency range of 1–100 kHz at different temperatures, as shown in Fig. 3. The ε' variation with increasing temperature was observed to increase, which could be due to the thermally activated charge carriers and increased polarization mechanisms.

Fig. 3 indicates that ε' grows monotonically with temperature up to a broad maximum and diminishes at higher temperature, displaying the characteristic dielectric relaxation of ferrites. At low temperature, charge carriers do not have enough vigor to accompany the reversing field, and thus small ε' is obtained. When temperature grows, thermal excitation favors $Fe^{2+} \leftrightarrow Fe^{3+}$ hopping and interfacial polarization near semiconducting grain and insulating grain boundaries (Maxwell–Wagner effect), giving rise to the ε' growth [32]. After the broad maximum, the downtrend is due to thermal agitation, which disarrays dipolar alignment and enhances leakage loss. Normal dielectric dispersion is observed in the frequency dependence, such that ε' diminishes with frequency rise due to fast oscillating field, which inhibits dipolar reorientation. Zn^{2+} substitution effect is prominent: ε' grows up to x ~ 0.8 Fig. 3c, owing to higher occupation of octahedral positions for Fe^{3+} and higher hopping polarization, yet diminishes for x ≥ 1.2 as shows Fig. 3e and 3f, due to non-magnetic Zn^{2+} ions, which disarrays the hoping network. such behavior is consistent with previous result for Zn-subsituted ferrite, confirming that cation redistribution and interfacial effected polarization control the dielectric response. One possible explanation for the rising trend of the dielectric constant ε' with increasing temperature is an increase in thermally activated charge carriers [33,37]. At elevated temperatures, the dielectric constant increased significantly, and was approximately 20–30 % higher than

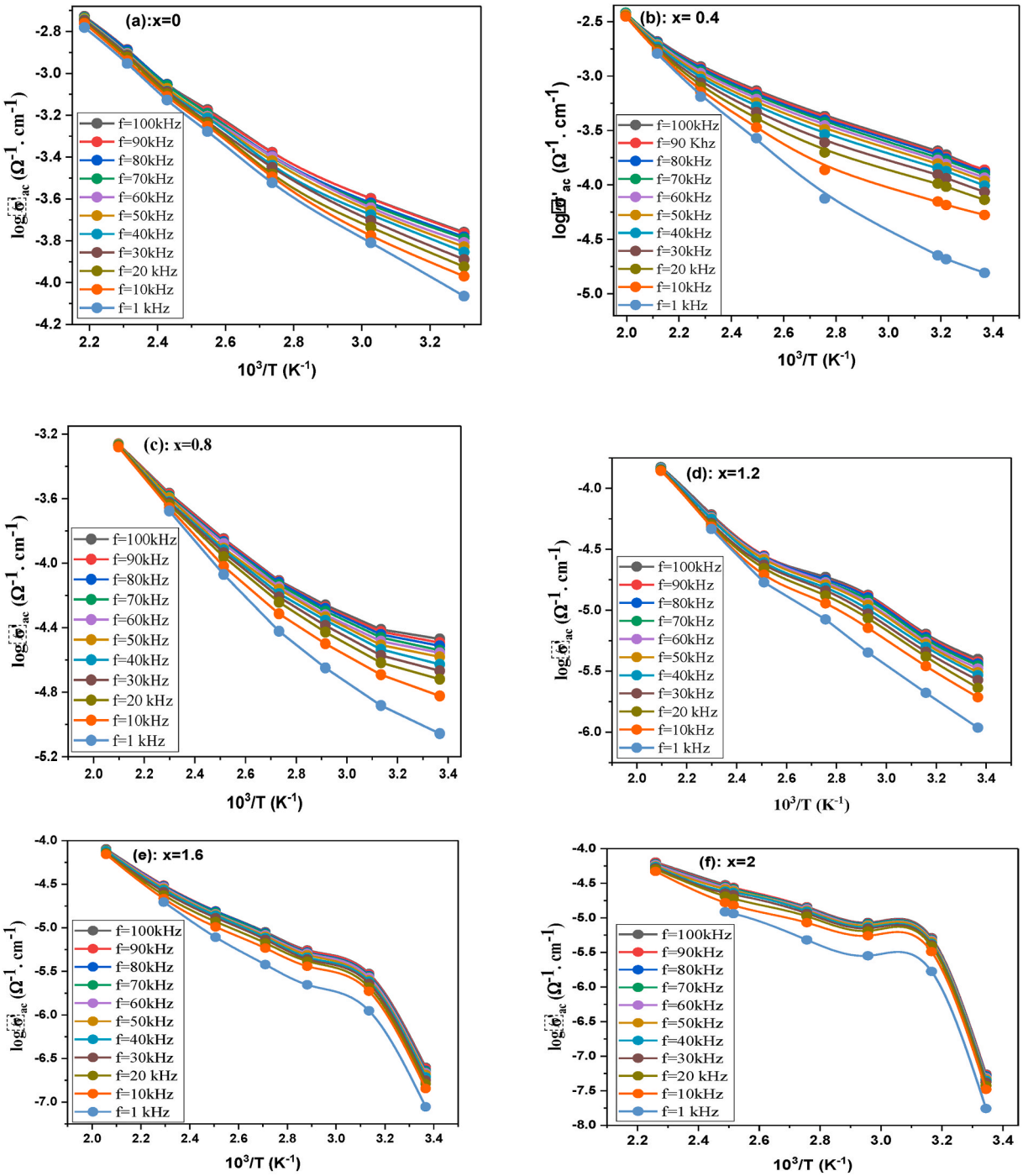

Fig. 2. AC conductivity as log σ_{ac} vs reciprocal temperature 1000/T of the $BaNi_{2-x}Zn_xFe_{16}O_{27}$, across different frequencies for (a) x = 0.0, (b) x = 0.4, (c) x = 0.8, (d) x = 1.2, (e) x = 1.6, and (f) x = 2.0.

that at room temperature. This increase originates primarily from the increased mobility of charge carriers, leading to increased polarization through mechanisms such as orientational dipole polarization and space-charge polarization. The electron transfer between Fe^{2+} and Fe^{3+} also contributes significantly to this effect, particularly in p-type ferrites, where electron transfer is more dominant than hole transfer at lower temperatures [38]. As a result, the polarization at reduced temperatures is weak because the dipoles, which are incapable of rapid rotation, oscillate under the effect of the field. When heating was applied and the temperature increased, the bound charge carriers acquired sufficient energy for thermal excitation, which increased the polarization and consequently increased the dielectric constant. In addition, from the variation in the dielectric constant with temperature, the dielectric constant increased with increasing temperature, which may be attributed to an increase in the molecular orientation and rearrangement with increasing temperature. However, the dielectric constant decreases at lower temperatures because of the reduction in the polarization strength [37]. The mobility of dipoles is low; hence, they cannot easily reorient themselves in an applied electric field. If the temperature increases, thermal excitation energy is provided to the bound charge carriers, enabling them to overcome this limitation, increasing the molecular orientation and rearrangement, and thus, further increasing the dielectric constant.

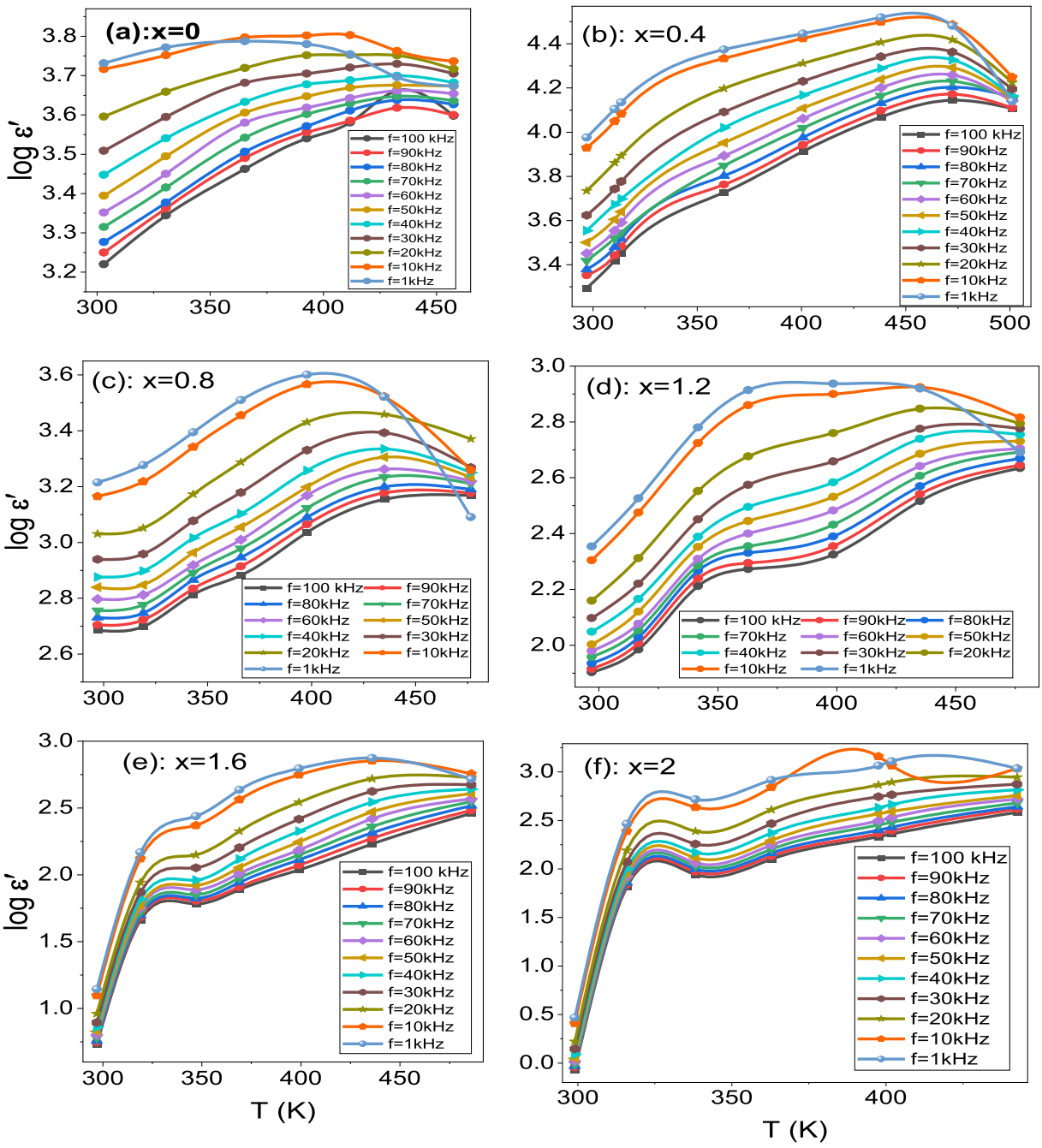

Fig. 3. Real part of the complex permittivity as log(ε') versus T(K), of $BaNi_{2-x}Zn_xFe_{16}O_{27}$, across different frequencies for (a) x = 0.0, (b) x = 0.4, (c) x = 0.8, (d) x = 1.2, (e) x = 1.6, and (f) x = 2.0.

3.3. *Imaginary part of the complex permittivity (ε″)*

Imagination part of the complex permittivity (ε″) versus temperature and frequency is given in Fig. 4 for $BaNi_{2-x}Zn_xFe_{16}O_{27}$ (x = 0.0–2.0). There is an unmistakable increase in ε″ with temperature due to the increased mobility of charge carriers and thermally driven relaxation of dipoles and space charges. ε″ is small at low temperature due to insufficient energy of charge carriers for the defeat of grain-boundary barriers. With increasing temperature, thermal excitation enhances $Fe^{2+}\leftrightarrow Fe^{3+}$ hopping and interfacial (Maxwell–Wagner) polarization between semiconducting grains and electrically insulting grain boundaries, resulting in the high-rise observed above 400 K. This is typical for the thermally driven relaxation mechanisms usually observed in ferrites [39,40].

Dielectric loss (ε″) is low at low temperatures due to minimal conduction loss that scales with σ_{ac} c. With rising temperature, σ_{ac} is higher and conduction losses increase, leading to larger ε″ values, especially at low frequencies, due to space-charge polarization effects. At high frequencies, polarization mechanisms cannot keep up with fast oscillations of fields and ε″ becomes small in comparison [37,41]. The frequency-dependent Reduction in ε″ thus follows the Koops–Maxwell–Wagner model, wherein low-frequency loss is controlled by resistive grain boundaries and high-frequency loss is controlled by conductive grains.

Zn^{2+} substitution also changes the amplitude and slope of ε″-T, With higher Zn content, ε″ decreases with x up to ≈0.8 due to less availability of Fe^{2+}/Fe^{39} hopping pairs. At higher Zn content, x ≥ 1.2, ε″ increases again at high temperatures, implying that Zn^{2+} ions in tetrahedral

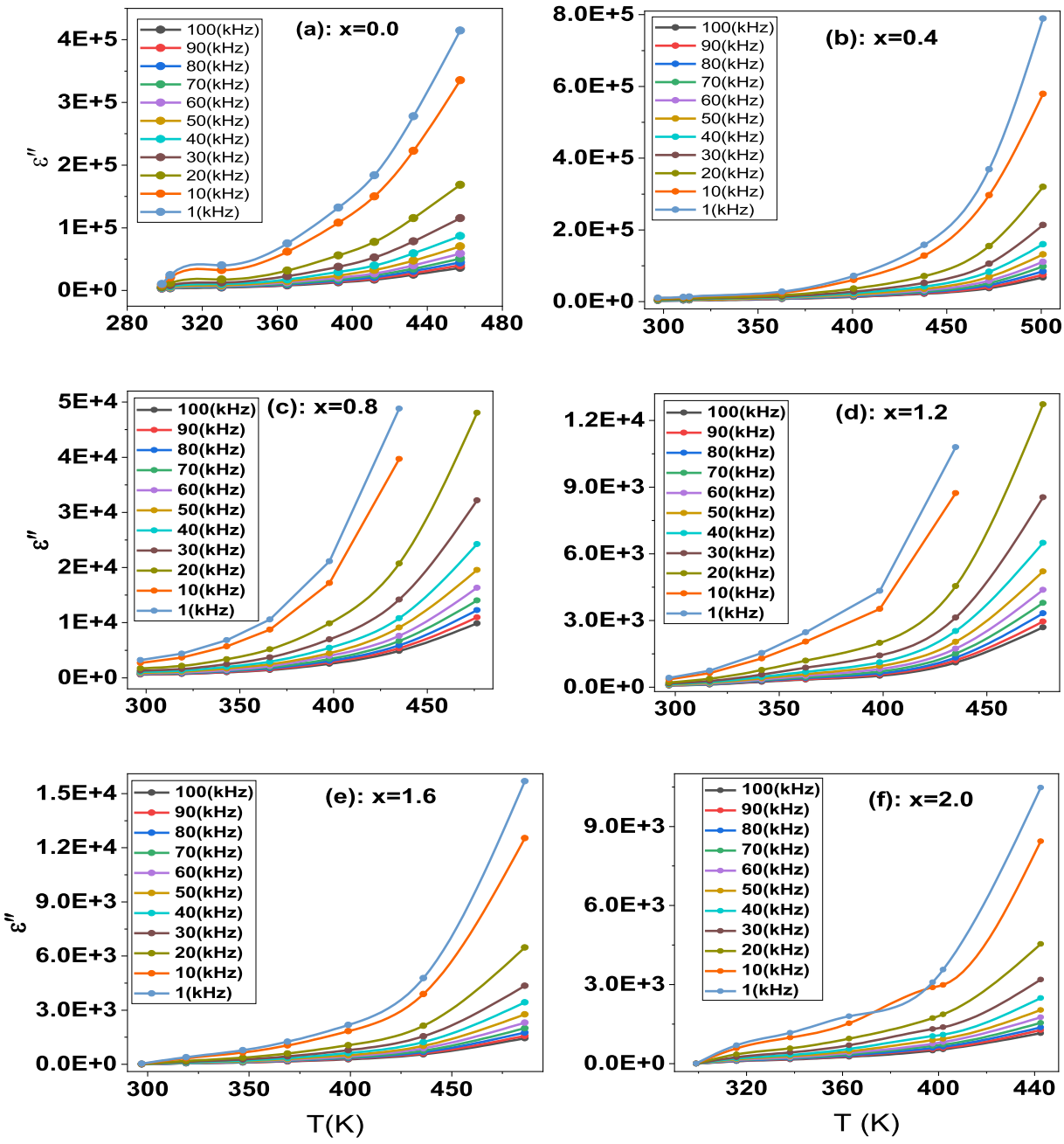

Fig. 4. Imaginary part of the complex permittivity (ε″) versus T(K) across different frequencies for $BaNi_{2-x}Zn_xFe_{16}O_{27}$, (a) x = 0.0, (b) x = 0.4, (c) x = 0.8, (d) x = 1.2, (e) x = 1.6, and (f) x = 2.0.

positions create lattice distortion and defects and increase local charge trap for enhancing losses. Minimum ε″ values in the intermediate temperature regime (x = 0.8–1.2) indicate points in the composition space where polarization and conduction losses are best balanced.

Generally, frequency- and temperature-dependent nature of ε″ validates that the dielectric losses in $BaNi_{2-x}Zn_xFe_{16}O_{27}$ follow thermally activated hopping conduction and interfacial polarization. With these features and the Zn-control, the oxide is promising for applications in high-temperature electronics, microwave absorbments, and energy storage [39].

3.4. Loss tangent

This study also analyzed the loss tangent (tan δ) of Zn-doped ferrites in relation to the temperature and frequency, revealing key insights into their dielectric relaxation processes. The results in Fig. 5 show that tan δ increases with temperature owing to enhanced dielectric absorption, which is a consequence of the thermal activation of charge carriers. The enhanced mobility of charge carriers at higher temperatures results in a higher energy dissipation as heat during polarization in the case of an alternating electric field. The same temperature dependence was observed by El Ata et al. [42]. This is because of the increased dielectric absorption owing to the thermal activation processes. This indicates that the charge carrier mobility increases with temperature; thus, more energy is dissipated as heat in polarization under an alternating electric field. The increase in tan δ with temperature is due to the increasing number of conduction electrons and their ability to allow more energy absorption and translation into heat owing to polarization [43,44]. The tan δ value increased more intensely at lower frequencies, which suggests that the action of lower frequency fields provides sufficient time for

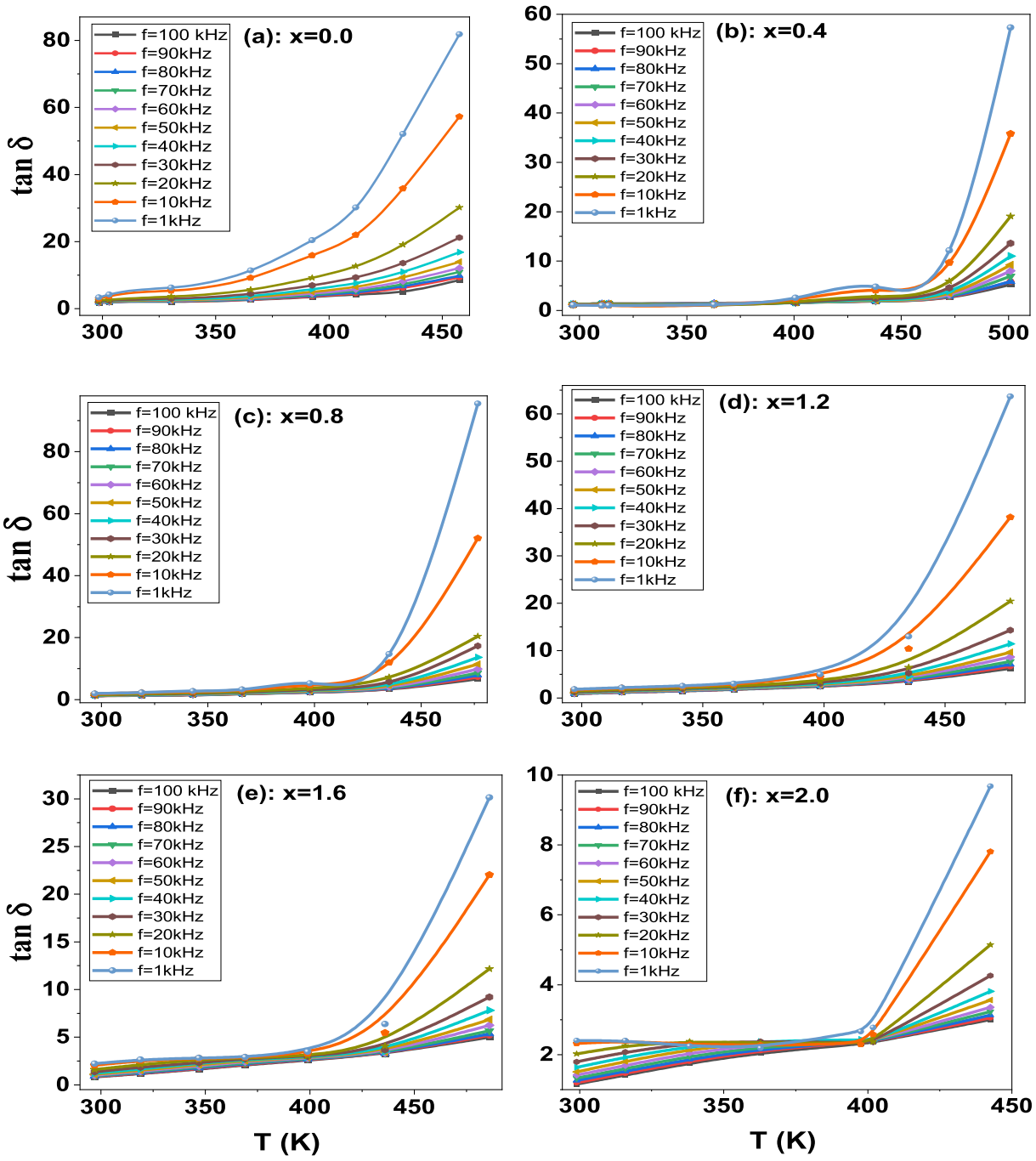

Fig. 5. Loss tangent (tan δ) versus T(K) for $BaNi_{2-x}Zn_xFe_{16}O_{27}$: (a) x = 0.0, (b) x = 0.4, (c) x = 0.8, (d) x = 1.2, (e) x = 1.6, and (f) x = 2.0, across different frequencies.

dipolar relaxation mechanisms to occur. The rate of increase in tan δ with temperature at lower frequencies is more intense because lower-frequency fields provide ample time for dipolar relaxation mechanisms to occur. However, at higher frequencies, tanδ decreases because the polarization is unable to keep up with the external electric field, which changes rapidly. The tan δ spectrum peaks for x = 1.6, Fig. 5e, and x = 2.0 Fig. 5f, are broad and indicate complex dielectric behavior and frequency-dependent relaxation processes. The peaks shift to higher temperatures with increasing frequency, indicating the capability of the material to ensure dielectric stability over a broad range of operating conditions. This is important for the optimization of Zn-doped ferrites for high-temperature and high-frequency applications, including capacitors, RF circuits, and industrial heating. The peaks are attributed to the relaxation mechanisms of dipolar and space charge polarization, and can provide insight into the manner in which doping levels should be adjusted to minimize dielectric losses and thus ensure high efficiency. The behavior, as seen from the increase in tan δ at higher temperatures and its reduction at higher frequencies, agrees with that of hexagonal ferrites such as $BaCo_{2-x}Ni_xFe_{16}O_{27}$ [42]. This indicates a high degree of correlation between the charge-carrier motion and external electric field. The coincidence of the transition temperature in σac with the broad peaks in tan δ indicates the interdependence of conduction and dielectric properties. This further suggests that charge carrier mobility and relaxation are intimately connected and can be achieved through controlled doping levels and operating conditions. These features provide stable operation over a wide range of temperatures and frequencies,

making them extremely useful for high-frequency electronics, low-power devices, and high-temperature applications, such as capacitors, RF circuits, and industrial heating. The variation in the dielectric loss tangent (tan δ) is associated with the ability of the charge carriers to follow an externally applied electric field. The observed decrease in tan δ at higher frequencies arises because the polarization mechanism cannot respond sufficiently rapidly to the alternating field beyond a certain frequency. Conversely, the increase in tan δ at elevated temperatures is attributed to the enhanced hopping frequency of the charge carriers, which facilitates greater energy dissipation within the material.

3.5. Composition dependent of σ_{ac}, ε', and tanδ

The influence of Zn substitution on the AC electrical conductivity, real part of the dielectric constant ε', and loss tangent was investigated, and the corresponding results are presented in Fig. 6. As shown in Fig. 6a, the variation in AC conductivity σ_{ac} with Zn content exhibits a behavior similar to that of the dielectric constant (ε') displayed in Fig. 6b, indicating that both AC conductivity and dielectric behavior originate from related polarization and charge transport mechanisms. The electrical conductivity and dielectric constant of the ferrite samples increased with Zn substitution up to x = 0.4, beyond which they exhibited a gradual decline, suggesting that excessive Zn content disrupted the optimal cation distribution responsible for charge hopping. The observed trend is in good agreement with the behavior reported in the literature for similar systems [25,34,45–47].

Cation distributions in $BaNi_{2-x}Zn_xFe_{16}O_{27}$ ferrites were derived from XRD intensity ratio analysis using the Bertaut method [31], which compares observed and calculated peak intensities:

$$\frac{I^{Obs.}_{hkl}}{I^{Obs.}_{h'k'l'}} \propto \frac{I^{Cal.}_{hkl}}{I^{Cal.}_{h'k'l'}} \quad (2)$$

Here, I^{Obs} and I^{Calc} denote the observed and calculated intensities, respectively, for the given (hkl) planes.

The resulting cation occupancies are presented in Table 2. The cation distribution data in Table 2 provide the structural basis for these observations. With increasing Zn substitution, Zn^{2+} ions progressively occupy the tetrahedral (A) site, displacing Fe^{3+}, while Ni^{2+} concentration at the octahedral (B) site decreases from 2.0 to 0.0 as Fe^{3+} content at B increases correspondingly (8.0 → 10.0). At low Zn levels (x ≤ 0.4), the modest increase in B-site Fe enhances the Fe–O–Fe linkages, facilitating Fe^{2+}/Fe^{3+} small-polaron hopping, thereby increasing σ and ε'. Such site-occupancy trends are consistent with recent reports on Zn-substituted ferrites [48]. At higher Zn substitution (x ≥ 0.4), although the B-site Fe content continued to increase, the depletion of Ni^{2+} and reduction of A-site Fe weakened the A–B superexchange pathways and reduced the

Table 2
Cation distribution for $BaNi_{2-x}Zn_xFe_{16}O_{27}$ ferrite.

Sample	Cation distribution	
	Tetrahedral (A-site)	Octahedral (B-site)
$BaNi_{2.0}Fe_{16}O_{27}$	$(BaZn_{0.0}Fe_{8.0})$	$[Ni_{2.0}Fe_{8.0}]$
$BaNi_{1.6}Zn_{0.4}Fe_{16}O_{27}$	$(BaZn_{0.4}Fe_{7.6})$	$[Ni_{1.6}Fe_{8.4}]$
$BaNi_{1.2}Zn_{0.4}Fe_{16}O_{27}$	$(BaZn_{0.8}Fe_{7.2})$	$[Ni_{1.2}Fe_{8.8}]$
$BaNi_{0.8}Zn_{1.2}Fe_{16}O_{27}$	$(BaZn_{1.2}Fe_{6.8})$	$[Ni_{0.8}Fe_{9.2}]$
$BaNi_{0.4}Zn_{1.6}Fe_{16}O_{27}$	$(BaZn_{1.6}Fe_{6.4})$	$[Ni_{0.4}Fe_{9.6}]$
$BaZn_{2.0}Fe_{16}O_{27}$	$(BaZn_{2.0}Fe_{6.0})$	$[Ni_{0.0}Fe_{10.0}]$

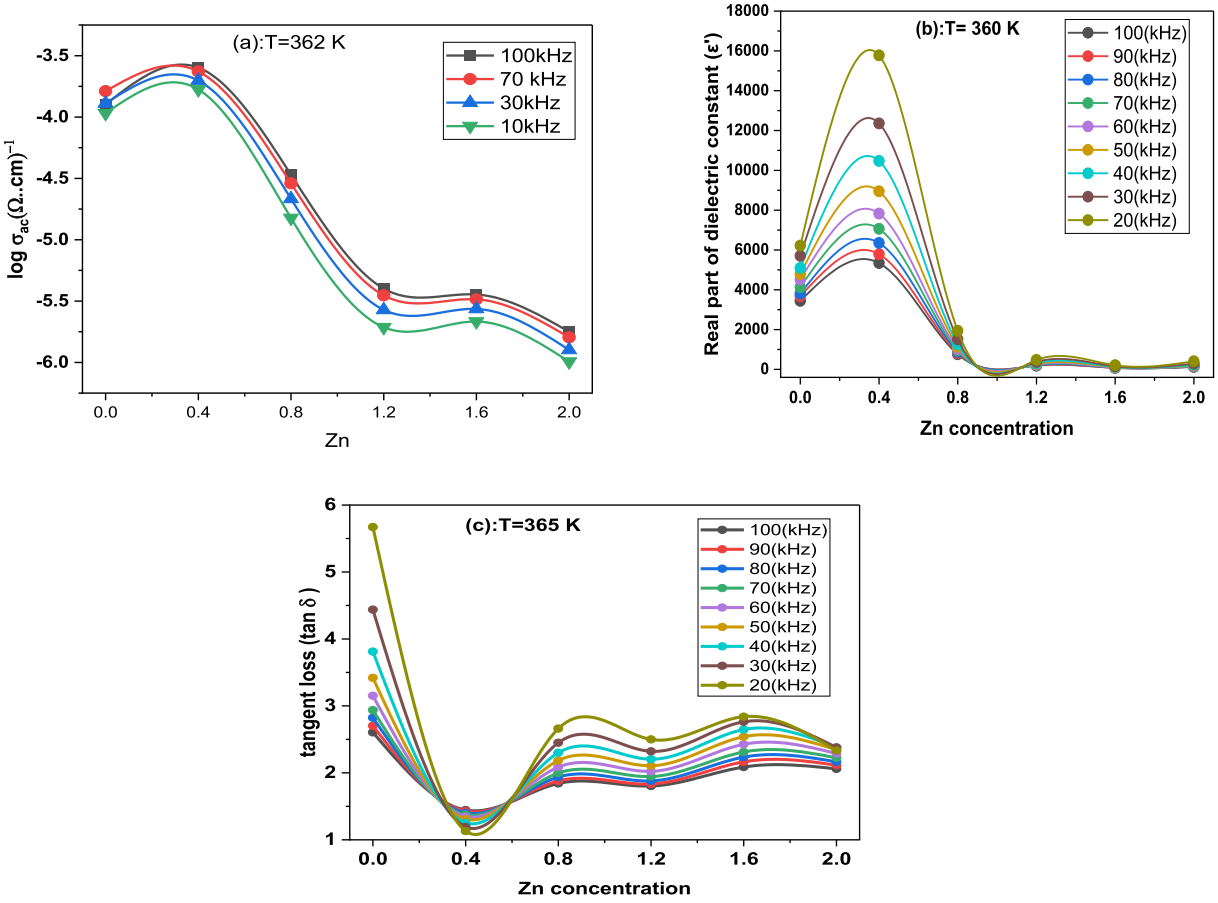

Fig. 6. Composition dependent of (a): electrical conductivity (σ_{ac}), (b): real part of dielectric constant (ε'), and (c): tangent loss (tan δ), at selected temperatures and frequencies.

polarization efficiency. Thus, the observed rise and subsequent decrease in the electrical conductivity and dielectric constant can be rationalized as the outcome of this cation redistribution, which modulates both the hopping probability and dielectric polarization [49].

The initial increase can therefore be related to electron hopping between Fe^{2+} and Fe^{3+} ions, which enhances charge transfer and increases the conductivity and polarization. This interpretation aligns with hopping models for ferrites [50]. However, the subsequent decrease in electrical and dielectric properties with further Zn substitution can be understood based on the replacement of magnetic Ni^{2+} ions by nonmagnetic Zn^{2+} ions at the A-sites, thereby reducing the polarization within the lattice. The co-presence of both Fe^{2+} and Fe^{3+} ions on the B-sites favors conduction via an electron exchange mechanism. In contrast, the presence of Zn^{2+} on A-sites reduces the population of Ni^{2+}, thereby lowering the probability of hole hopping between Ni^{2+}–Ni^{3+} pairs and weakening the polarization. Accordingly, the electrical conductivity shows a corresponding reduction with a decrease in the dielectric constant.

Fig. 6b shows the dielectric constant, which strongly depends on the level of Zn substitution. The dielectric constant increased with increasing Zn content and reached a maximum at $x = 0.4$. This is indicative of improved dielectric properties at this doping level, possibly owing to enhanced polarization mechanisms under optimal structural and electronic arrangements [46,47,51]. When $x > 0.4$, it decreases and stabilizes at smaller values, as shown in Fig. 6b. This decrease indicates that excess Zn addition might disturb the dielectric mechanism of this ferrite system; structural distortion or modified dynamics of the charge carriers could be responsible for this effect. These findings agree well with previously reported studies related to the sensitivity of ferrites to compositional aspects with respect to their dielectric behavior [52,53].

The variation in the dielectric loss tangent (tan δ) confirms the results described above for the dielectric constant. The loss tangent decreased as Zn substitution increased to a minimum value at $x = 0.4$, reflecting a minimum energy dissipation and a better dielectric efficiency at this substitution rate, as shown in Fig. 6c. Beyond this rate, for $x > 0.4$, the loss tangent increased, indicating deterioration of the dielectric properties. This increase may be attributed to microstructural changes or the saturation of benefits provided by the addition of Zn, as indicated by other reports on Zn-substituted ferrites [46,54]. The low loss factor observed at $x = 0.4$ is especially desirable in applications involving capacitors and other electronic devices with high dielectric efficiency, as shown in Fig. 6c.

These results establish $x = 0.4$ as the optimum substitution level at which the dielectric constant reaches a maximum, tan δ reaches a minimum, and σac reaches its maximum value. The obtained results confirm that moderate Zn doping enhances polarization, reduces energy dissipation, and improves charge-carrier mobility via mechanisms such as small-polaron hopping. These findings highlight the flexibility and adaptability of Zn-doped ferrites in advanced applications. The optimized properties at $x = 0.4$ make such materials highly suitable for RF and microwave devices, capacitors, and energy storage systems where stable dielectric performance and efficient conductivity are essential.

3.6. XRD analysis

X-ray diffraction (XRD) analysis was also performed to confirm the formation of the crystalline phase, lattice parameters, and any secondary phases. According to the XRD results in Refs. [27,55] The XRD patterns in Fig. 7 confirm the formation of a single-phase W-type hexaferrite structure, as provided by the c/a ratio value, without detectable secondary phases, indicating the successful incorporation of Zn into the Ni–Ba ferrite matrix. Based on the Scherrer formula [55], the grain size

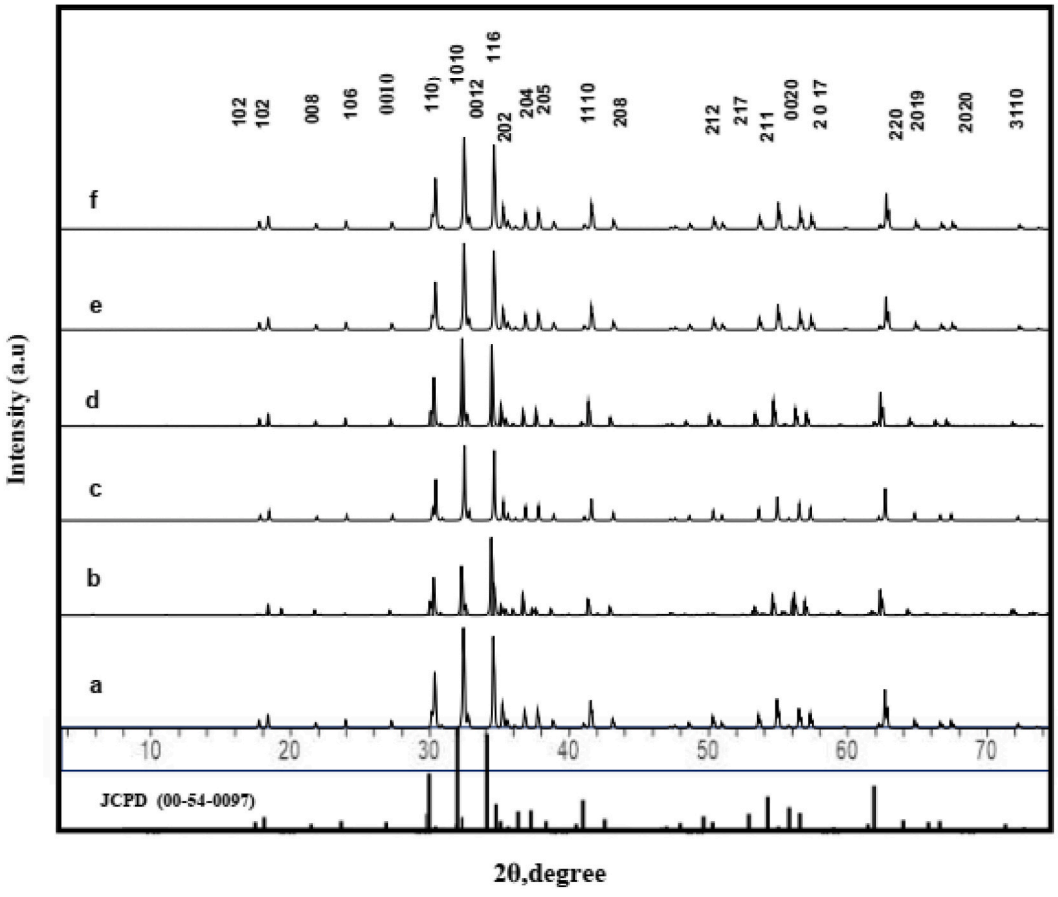

Fig. 7. XRD patterns of $BaNi_{2-x}Zn_xFe_{16}O_{27}$ ferrites sample for (a): $x = 0.0$, (b): $x = 0.4$, (c): $x = 0.8$, (d): $x = 1.2$, (e): $x = 1.6$, and (f): $x = 2.0$.

was estimated to be in the nanometer range (35–37 nm). The lattice constant and AC volume of the unit cell were calculated based on equations (3) and (4). The refined lattice constants (*a* and *c*) and corresponding unit cell volumes in Table 3 exhibit a gradual increase with Zn substitution, consistent with the replacement of Ni^{2+} (ionic radius 0.69 Å) by the larger Zn^{2+} ions (0.74 Å). The increase in the unit cell volume from 991.944 $Å^3$ (x = 0) to 1025.005 $Å^3$ (x = 2.0) further confirmed Zn incorporation of Zn. The absence of impurity peaks validates the high phase purity of the samples, whereas the observed lattice expansion directly correlates with the compositional dependence of the electrical and dielectric properties [27].

Physical structural properties such as density and porosity were calculated using equations (5a), (5b) and (6), respectively. The results in Table 3 demonstrate a decrease in density as Zn substitution increases, while the percent porosity correspondingly increases from 11.2 % at x = 0–20.9 % at x = 2.0. This trend indicates that a higher Zn content inhibits densification during sintering, resulting in greater pore formation [56]. Such microstructural changes strongly influence the dielectric and conductivity behavior; higher porosity and larger grains reduce the effective conduction pathways and suppress polarization, which is consistent with the observed decrease in the dielectric constant and AC conductivity at higher Zn levels (Fig. 6a and b).

$$\frac{1}{d_{hkl}^2}=\frac{4}{3}\frac{h^2+hk+k^2}{a^2}+\frac{L^2}{C^2} \tag{3}$$

$$V_{cell}=a^2c\,Sin\,(120^\circ). \tag{4}$$

$$\rho_B=\frac{m}{\pi\, r^2 h} \tag{5;a}$$

$$\rho_x=\frac{ZM}{N_A V} \tag{5;b}$$

$$\%P=\left(\frac{\rho_{x-}\rho_B}{\rho_x}\right)\times 100 \tag{6}$$

Importantly, the moderate expansion observed at **x = 0.4** corresponds to the composition where the electrical conductivity and dielectric constant reach their maximum, as shown in Fig. 6a and b, indicating that subtle lattice modifications at this substitution level optimize polarization mechanisms. Overall, the XRD-confirmed lattice expansion with Zn substitution directly correlates with the observed trends in dielectric and conductivity behavior, where moderate substitution (x ≈ 0.4) optimizes polarization and charge transport, whereas higher Zn levels introduce porosity and disorder that suppress electrical performance.

4. Conclusion

In this study, $BaNi_{2-x}Zn_xFe_{16}O_{27}$ ferrites were synthesized successfully by the ceramic method, and their electrical and dielectric properties were systematically investigated as a function of Zn substitution. These results provide significant insights into their behavior and applications. Electrical and dielectric measurements demonstrated that the conductivity and dielectric constant increased with temperature up to a transition point (Tσ), beyond which thermal disorder suppressed carrier orientation. Importantly, the composition at x = 0.4 exhibited the most favorable combination of properties of high dielectric constant, maximum AC conductivity, and minimum dielectric loss, highlighting the role of moderate Zn substitution in enhancing polarization and charge carrier mobility. In contrast, higher Zn levels (x ≥ 1.6) introduced structural disorder and porosity, which suppressed both the conductivity and the dielectric response. These findings highlight the promising versatility and adaptability of Zn-doped ferrites in new applications. The optimized x = 0.4 characteristics make the materials highly suitable for RF and microwave devices, capacitors, and energy storage systems where stable dielectric behavior and good conductivity are paramount. The x = 1.6 and x = 2 behaviors also offer opportunities for materials tailoring for high-temperature and frequency-dependent applications, and the integration of structural, microstructural, and electrical results demonstrates a direct structure–property relationship, with x = 0.4 identified as an optimum composition. XRD analysis confirmed the formation of a single-phase W-type hexaferrite structure, with lattice parameters and unit cell volume V expansion gradually due to the substitution of Ni^{2+} by larger Zn^{2+} ions, which directly correlates with the observed trends in dielectric and conductivity behavior. Microstructural analysis further revealed an increase in porosity and a slight increase in grain size with higher Zn content, which strongly influenced the charge transport and dielectric polarization.

Zn substitution optimizes dielectric and electrical performance in $BaNi_{2-x}Zn_xFe_{16}O_{27}$, at x = 0.4 by enhancing B-site Fe^{2+}/Fe^{3+} hopping, making these ferrites highly attractive for RF/microwave devices, capacitors, and energy-storage applications requiring high polarization efficiency and low dielectric loss. This work provides new insights into tailoring ferrite compositions for targeted performance, offering potential applications in RF/microwave devices, capacitors, energy-storage systems, and high-temperature frequency-sensitive components. These findings highlight the novelty of compositionally driven optimization in W-type ferrites, bridging fundamental mechanisms with technological relevance.

CRediT authorship contribution statement

Sadiq H. Khoreem: Writing – review & editing, Software, Methodology, Investigation, Formal analysis, Conceptualization. **A.H. Al-Hammadi:** Writing – original draft, Validation, Supervision, Resources, Data curation, Conceptualization.

Funding statement

'Not applicable'; No Founding.

Declaration of competing interest

The authors declare the following financial interests/personal relationships which may be considered as potential competing interests: Sadiq H. Khoreem reports a relationship with Al-Razi University; and Amran University that includes: non-financial support. If there are other authors, they declare that they have no known competing financial

Table 3
XRD parameters (lattice constants, axial ratio, unit cell volume, density, porosity, average grain size) for $BaNi_{2-x}Zn_xFe_{16}O_{27}$ ferrite samples.

Empirical Formula	Lattices constant (Å)		Axial ratio	Volume of unit cell ($Å^3$)	Density(g/cm^3)		Porosity	Grain Size (nm)
Sample	a	c	c/a	V_{cell}	ρ_{x-ray}	ρ_b	(*P* %)	D
$BaNi_2Fe_{16}O_{27}$	5.984	31.987	5.478	991.944	5.346	4.7463	11.217	35.64
$BaNi_{1.6}Zn_{0.4}Fe_{16}O_{27}$	5.976	32.742	5.478	1012.644	5.29	4.6255	12.5606	35.181
$BaNi_{1.2}Zn_{0.8}Fe_{16}O_{27}$	5.978	32.759	5.479	1013.848	5.249	4.5566	13.2041	35.531
$BaNi_{0.8}Zn_{1.2}Fe_{16}O_{27}$	5.982	32.785	5.480	1016.011	5.249	4.4165	15.8624	35.814
$BaNi_{0.4}Zn_{1.6}Fe_{16}O_{27}$	5.986	32.877	5.492	1020.225	5.243	4.1895	19.0982	36.376
$BaNi_2Fe_{16}O_{27}$	5.998	32.899	5.484	1025.005	5.216	4.1796	20.8684	36.664

interests or personal relationships that could have appeared to influence the work reported in this paper.A. H. Al-Hammadi reports a relationship with Sana'a University that includes: non-financial support. If there are other authors, they declare that they have no known competing financial interests or personal relationships that could have appeared to influence the work reported in this paper.

Data availability

Data will be made available on request.

References

[1] K.K. Kefeni, T.A.M. Msagati, B.B. Mamba, Ferrite nanoparticles: synthesis, characterisation and applications in electronic device, Mater. Sci. Eng., B 215 (2016) 37–55, https://doi.org/10.1016/j.mseb.2016.11.002.

[2] R.C. Pullar, Hexagonal ferrites: a review of the synthesis, properties and applications of hexaferrite ceramics, Prog. Mater. Sci. 57 (2012) 1191–1334, https://doi.org/10.1016/j.pmatsci.2012.04.001.

[3] H.-S. Cho, S.-S. Kim, The effect of Zn and Ni substitution on magnetic and microwave absorbing properties of Co2W hexagonal ferrites, Ceram. Int. 45 (2018) 9406–9409, https://doi.org/10.1016/j.ceramint.2018.08.178.

[4] J. Zhao, X. Zhang, S. Liu, W. Zhang, Z. Liu, Effect of Ni substitution on the crystal structure and magnetic properties of BiFeO3, J. Alloys Compd. 557 (2013) 120–123, https://doi.org/10.1016/j.jallcom.2013.01.005.

[5] D.A. Vinnik, A.S. Semisalova, L.S. Mashkovtseva, A.K. Yakushechkina, S. Nemrava, S.A. Gudkova, D.A. Zherebtsov, N.S. Perov, L.I. Isaenko, R. Niewa, Growth, structural and magnetic characterization of Zn-substituted barium hexaferrite single crystals, Mater. Chem. Phys. 163 (2015) 416–420, https://doi.org/10.1016/j.matchemphys.2015.07.059.

[6] B. Ünal, A. Baykal, Effect of Zn substitution on electrical properties of nanocrystalline cobalt ferrite, J. Supercond. Nov. Magnetism 27 (2013) 469–479, https://doi.org/10.1007/s10948-013-2285-2.

[7] S. Kumar, J. Prakash, A. Verma, R. Jasrotia, A comprehensive review of synthesis, properties, and applications of BaFe12O19 hexaferrites, Mater. Today Proc. (2023), https://doi.org/10.1016/j.matpr.2023.02.346.

[8] G.B. Todkar, M. Hadi, R.H. Kadam, S.E. Shirsath, A. Imran, R.N. Kamble, K. M. Batoo, E.H. Raslan, R.A. Kunale, M.F. Ijaz, Ce–Dy substituted barium hexaferrite nanoparticles with large coercivity for permanent magnet and microwave absorber application, J. Phys. D Appl. Phys. 54 (2021) 294001, https://doi.org/10.1088/1361-6463/abf864.

[9] F. Bibi, S. Iqbal, H. Sabeeh, T. Saleem, B. Ahmad, M. Nadeem, I. Shakir, M. Aadil, A. Kalsoom, Evaluation of structural, dielectric, magnetic and photocatalytic properties of Nd and Cu co-doped barium hexaferrite, Ceram. Int. 47 (2021) 30911–30921, https://doi.org/10.1016/j.ceramint.2021.07.274.

[10] F. Guo, G. Ji, J. Xu, H. Zou, S. Gan, X. Xu, Effect of different rare-earth elements substitution on microstructure and microwave absorbing properties of Ba0.9RE0.1Co2Fe16O27 (RE=La, Nd, Sm) particles, J. Magn. Magn Mater. 324 (2011) 1209–1213, https://doi.org/10.1016/j.jmmm.2011.11.011.

[11] K. Jyotsna, S. Phanjoubam, Improved magnetoelectric coupling of Co–Ti substituted barium hexaferrite at room temperature and related electrical investigations, Mater. Chem. Phys. 317 (2024) 129186, https://doi.org/10.1016/j.matchemphys.2024.129186.

[12] M. Ahmad, F. Aen, M.U. Islam, S.B. Niazi, M.U. Rana, Structural, physical, magnetic and electrical properties of La-substituted W-type hexagonal ferrites, Ceram. Int. 37 (2011) 3691–3696, https://doi.org/10.1016/j.ceramint.2011.06.031.

[13] S. He, S. He, S. He, L. Wang, B. Shen, B. Shen, B. Shen, X. Ye, B. Shen, R. Liu, X. Liu, Influences of divalent ion substitution on the magnetic and dielectric properties of W-type barium ferrite, Chin. Phys. B 33 (2024), https://doi.org/10.1088/1674-1056/ad39d5.

[14] A. Iqbal, M.A. Khan, R.T. Rasool, S. Gulbadan, M.M. Algaradah, G.A. Ashraf, T. Alshahrani, H.S.M. Abd-Rabboh, M.N. Akhtar, M. Irfan, Dielectric, reflection loss and physicochemical studies of Cr doped Ba–Sr based W type hexagonal ferrites for microwave absorption applications, Ceram. Int. 50 (2023) 4446–4461, https://doi.org/10.1016/j.ceramint.2023.11.163.

[15] C.D. Patel, P.N. Dhruv, S.S. Meena, C. Singh, S. Kavita, M. Ellouze, R.B. Jotania, Influence of Co4+-Ca2+ substitution on structural, microstructure, magnetic, electrical and impedance characteristics of M-type barium–strontium hexagonal ferrites, Ceram. Int. 46 (2020) 24816–24830, https://doi.org/10.1016/j.ceramint.2020.05.326.

[16] A. Sudhakaran, A. Sudhakaran, E. Sivasenthil, Comprehensive analysis of optical, dielectric, and electrical properties in Al- and Cu-Doped barium hexaferrite/cobalt–zinc ferrite hybrid nanocomposites, J. Electron. Mater. 53 (2024) 4622–4644, https://doi.org/10.1007/s11664-024-11197-4.

[17] C. Venkateshwarlu, C. Ashok, B.A. Rao, D. Ravinder, B.S. Boyanov, Electrical conductivity of Co–Zr substituted hexagonal barium ferrites, J. Alloys Compd. 426 (2006) 1–3, https://doi.org/10.1016/j.jallcom.2006.02.001.

[18] G. Mustafa, I. Bibi, F. Majid, M. Sultan, B. Taj, Z. Nazeer, H. Muhammad Umair, Z. M. Elqahtani, N. Alwadai, M.I. Khan, M. Iqbal, Zn and Ni doping effect on barium hexaferrite ferroelectric, optical properties and photocatalytic activity under visible light irradiation, Phys. B Condens. Matter 663 (2023) 415006, https://doi.org/10.1016/j.physb.2023.415006.

[19] N.F. Khatoon, A. Khan, Z. Aslam, M. Shoab, J. Ali, M. Zulfequar, Effect of Zn doping on structural, morphological, optical and electrical properties of Bi2Se3 material, Next Mater. 5 (2024) 100234, https://doi.org/10.1016/j.nxmate.2024.100234.

[20] D.A. Oeba, J.O. Bodunrin, S.J. Moloi, The electrical characteristics and conduction mechanisms of Zn doped silicon-based Schottky barrier diode, Heliyon 9 (2023) e22793, https://doi.org/10.1016/j.heliyon.2023.e22793.

[21] P. Vijaya Bhasker Reddy, B. Ramesh, C. Gopal Reddy, Electrical conductivity and dielectric properties of zinc substituted lithium ferrites prepared by sol–gel method, Phys. B Condens. Matter 405 (2010) 1852–1856, https://doi.org/10.1016/j.physb.2010.01.062.

[22] R.S. Rajenimbalkar, V.J. Deshmukh, K.K. Patankar, S.B. Somvanshi, Effect of multivalent ion doping on magnetic, electrical, and dielectric properties of nickel ferrite nanoparticles, Sci. Rep. 14 (2024), https://doi.org/10.1038/s41598-024-81222-3.

[23] A. Manohar, V. Vijayakanth, S.V. Prabhakar Vattikuti, K.H. Kim, Electrochemical investigation on nickel-doped spinel magnesium ferrite nanoparticles for supercapacitor applications, Mater. Chem. Phys. 301 (2023) 127601, https://doi.org/10.1016/j.matchemphys.2023.127601.

[24] R. Priyadharsini, C. Manoharan, M. Bououdina, S. Sagadevan, M. Venkateshwarlu, S. Asath Bahadur, Impact of nickel substitution on structural, dielectric, magnetic, and electrochemical properties of copper ferrite nanostructures for energy storage devices, J. Colloid Interface Sci. 653 (2023) 917–929, https://doi.org/10.1016/j.jcis.2023.09.113.

[25] P. Behera, S. Ravi, Effect of Ni doping on structural, magnetic and dielectric properties of M-type barium hexaferrite, Solid State Sci. 89 (2019) 139–149, https://doi.org/10.1016/j.solidstatesciences.2019.01.003.

[26] N. Dawar, I.S. Sandhu, J.S. Jolly, S. Malhotra, M. Chitkara, Structural, magnetic and dielectric properties of pure and nickel-doped barium nanohexaferrites synthesized using chemical co-precipitation technique, Cogent Physics 3 (2016), https://doi.org/10.1080/23311940.2016.1208450.

[27] S.H. Khoreem, A.H. Al-Hammadi, Enhancing optical properties of Ba-Ni ferrite through nonmagnetic ion doping for sustainable green technologies and renewable energy applications, Discov Sustain 5 (2024), https://doi.org/10.1007/s43621-024-00559-x.

[28] G.N. Rajivgandhi, G. Ramachandran, C.C. Kanisha, N.S. Alharbi, S. Kadaikunnan, J.M. Khaled, K.F. Alanzi, W.-J. Li, Effect of Ti and Cu doping on the structural, optical, morphological and anti-bacterial properties of nickel ferrite nanoparticles, Results Phys. 23 (2021) 104065, https://doi.org/10.1016/j.rinp.2021.104065.

[29] I. Cinar, Improving structural and magnetic properties of zinc stannate thin films through nickel doping via sol–gel method, Sci. Rep. 14 (2024), https://doi.org/10.1038/s41598-024-63209-2.

[30] H. Himanshi, R. Jasrotia, J. Prakash, R. Verma, P. Thakur, A. Kandwal, F. Wan, A. Thakur, Synthesis, characterization, and applications of doped barium hexaferrites: a review, Phys. B Condens. Matter 667 (2023) 415202, https://doi.org/10.1016/j.physb.2023.415202.

[31] A. Ghasemi, A. Hossienpour, A. Morisako, A. Saatchi, M. Salehi, Electromagnetic properties and microwave absorbing characteristics of doped barium hexaferrite, J. Magn. Magn Mater. 302 (2005) 429–435, https://doi.org/10.1016/j.jmmm.2005.10.006.

[32] A.M. Abo El Ata, M.K. El Nimr, S.M. Attia, D. El Kony, A.H. Al-Hammadi, Studies of AC electrical conductivity and initial magnetic permeability of rare-earth-substituted Li–Co ferrites, J. Magn. Magn Mater. 297 (2005) 33–43, https://doi.org/10.1016/j.jmmm.2005.01.085.

[33] M.A. Ahmed, N. Okasha, R.M. Kershi, Dramatic effect of rare earth ion on the electrical and magnetic properties of W-type barium hexaferrites, Phys. B Condens. Matter 405 (2010) 3223–3233, https://doi.org/10.1016/j.physb.2010.04.047.

[34] D.J. Sánchez-Trujillo, L.V. Osorio-Maldonado, J.J. Prías-Barragán, Temperature dependence of electrical conductivity and variable hopping range mechanism on graphene oxide films, Sci. Rep. 13 (2023), https://doi.org/10.1038/s41598-023-31778-3.

[35] C. Tsonos, Comments on frequency dependent AC conductivity in polymeric materials at low frequency regime, Curr. Appl. Phys. 19 (2019) 491–497, https://doi.org/10.1016/j.cap.2019.02.001.

[36] X. Xia, Y. Wang, Z. Zhong, G.J. Weng, A frequency-dependent theory of electrical conductivity and dielectric permittivity for graphene-polymer nanocomposites, Carbon 111 (2016) 221–230, https://doi.org/10.1016/j.carbon.2016.09.078.

[37] P.K. Singh, S.K. Tripathi, S.K. Sharma, D.K. Dwivedi, Study of dielectric relaxation and thermally activated a.c. conduction in multicomponent Ge10−xSe60Te30Inx ($0 \leq x \leq 6$) chalcogenide glasses using CBH model, Results Phys. 12 (2018) 223–236, https://doi.org/10.1016/j.rinp.2018.11.048.

[38] M.K. Vishwakarma, P. Jain, Investigation of temperature-activated charge-carrier dynamics and dielectric relaxation in Fe, Cu–Doped CeO_2, Phys. Status Solidi 220 (2023), https://doi.org/10.1002/pssa.202300349.

[39] V.N. Hegde, V.V. Manju, B.C. Hemaraju, Frequency and temperature dependent dielectric properties of CuO nanoparticles, Chem. Phys. Impact 8 (2024) 100474, https://doi.org/10.1016/j.chphi.2024.100474.

[40] M.A. Darwish, S.A. Saafan, E.L. Trukhanova, A.S.B. Sombra, D. Zhou, C. Singh, A. T. Morchenko, K.A. Astapovich, O.S. Senatov, R.B. Jotania, A.V. Trukhanov, A. A. Pilyushkin, S.V. Trukhanov, Investigation of AC-Measurements of epoxy/ferrite composites, Nanomaterials 10 (2020) 492, https://doi.org/10.3390/nano10030492.

[41] N. Chandel, M.M.A. Imran, N. Mehta, Comprehensive studies of temperature and frequency dependent dielectric and a.c. conducting parameters in third generation

multi-component glasses, RSC Adv. 8 (2018) 25468–25479, https://doi.org/10.1039/c8ra04214d.
[42] A.M. Abo El Ata, M.K. El Nimr, D. El Kony, A.H. Al-Hammadi, Dielectric and magnetic permeability behavior of BaCo 2− xNi xFe 16O 27 W-type hexaferrites, J. Magn. Magn Mater. 204 (1999) 36–44, https://doi.org/10.1016/s0304-8853(99)00381-9.
[43] A. Tataroglu, H. Durmuş, A.F. Vahid, B. Avar, Ş. Altındal, High-temperature sensitivity complex dielectric/electric modulus, loss tangent, and AC conductivity in Au/(S:DLC)/p-Si (MIS) structures, J. Mater. Sci. Mater. Electron. 35 (2024), https://doi.org/10.1007/s10854-024-12007-7.
[44] K. Pubby, S.K. Chawla, R.K. Mudsainiyan, S.B. Narang, Effect of temperature on dielectric and electrical properties of Co–Zr doped barium hexaferrites prepared by sol–gel method, J. Mater. Sci. Mater. Electron. 27 (2016) 11220–11230, https://doi.org/10.1007/s10854-016-5242-6.
[45] A.M. Abdeen, Electric conduction in Ni–Zn ferrites, J. Magn. Magn Mater. 185 (1998) 199–206, https://doi.org/10.1016/s0304-8853(97)01144-x.
[46] R.J. Pandya, U.S. Joshi, O.F. Caltun, Microstructural and electrical properties of barium strontium titanate and nickel zinc ferrite composites, Procedia Mater. Sci. 10 (2015) 168–175, https://doi.org/10.1016/j.mspro.2015.06.038.
[47] J. Ferdaus, M.K. Das, A. Dey, B.C. Das, F. Alam, M. Rahaman, M.A. Hoque, M. S. Bashar, Influence of Zn-substitution on structural, magnetic, dielectric, and electric properties of Li–Ni–Cu ferrites, Heliyon 9 (2023) e21633, https://doi.org/10.1016/j.heliyon.2023.e21633.
[48] C. Murugesan, L. Okrasa, K. Ugendar, G. Chandrasekaran, X. Liu, D. Diao, J. Shen, Improved magnetic and electrical properties of Zn substituted nanocrystalline MgFe2O4 ferrite, J. Magn. Magn Mater. 550 (2022) 169066, https://doi.org/10.1016/j.jmmm.2022.169066.
[49] M.A. El Hiti, Dielectric behaviour in Mg–Zn ferrites, J. Magn. Magn Mater. 192 (1999) 305–313, https://doi.org/10.1016/s0304-8853(98)00356-4.
[50] P.V. Reddy, T.S. Rao, Electrical conductivity of lithium-nickel ferrites, J. Less Common Met. 79 (1981) 191–198, https://doi.org/10.1016/0022-5088(81)90067-9.
[51] P. Kishan, D.R. Sagar, P. Swarup, Electrical conduction and dielectric behaviour in zinc-substituted lithium ferrites, J. Less Common Met. 108 (1985) 345–351, https://doi.org/10.1016/0022-5088(85)90229-2.
[52] D. Wang, X. Liu, K. Ge, Y. Zou, Z. Wang, Z. Feng, G. Duan, J. Du, H. Wu, Effects of Zn2+ substitution on the dielectric properties, chemical bonding properties, and crystal structure of Mg3(PO4)2 ceramics, Ceram. Int. 50 (2024) 36220–36229, https://doi.org/10.1016/j.ceramint.2024.07.006.
[53] L. Huang, The effect of Zn doping on the structure, phase transformation and electric properties of 0.5BZT-0.5BCT materials, Heliyon 10 (2024) e33845, https://doi.org/10.1016/j.heliyon.2024.e33845.
[54] J. Parashar, J. Jyoti, V.K. Saxena, D. Bhatnagar, K.B. Sharma, Dielectric behaviour of Zn substituted Cu nano-ferrites, J. Magn. Magn Mater. 394 (2015) 105–110, https://doi.org/10.1016/j.jmmm.2015.06.044.
[55] S.H. Khoreem, A.H. Al-Hammadi, Studies on the electrical and optical conductivity of barium-nickel ferrite nanoparticles doped with Zn, Discover Nano 20 (2025), https://doi.org/10.1186/s11671-024-04180-9.
[56] S.H. Khoreem, A.A.M. Othman, A.H. Al-Hammadi, Enhancing dielectric permittivity in barium ferrite: a novel material for energy storage and advanced electronics applications, Discov. Appl. Sci. 7 (2025), https://doi.org/10.1007/s42452-025-06801-z.